

# HBAR as a High Frequency High Stress Generator

Tanay A. Gosavi, Evan R. MacQuarrie  
and Gregory D. Fuchs  
Cornell University  
Ithaca, NY, USA  
tag75@cornell.edu

Sunil A. Bhawe  
Purdue University  
West Lafayette, IN, USA  
bhave@purdue.edu

**Abstract**— In this paper we report on High-Overtone Bulk Acoustic Resonator (HBAR) as high stress generator by measuring f-Q product of various tones and overtones from room temperature to 80 Kelvin. HBARS provide excellent acoustic isolation from anchor losses as the modes are confined within the high finesse acoustic cavity made from single crystal diamond or silicon carbide (SiC) substrates. Their high Q and linearity makes them robust transducers for generating up to 20MPa AC stress with small drive voltages at GHz frequencies which is instrumental in manipulating spin-defect qubits in these materials.

**Keywords**—HBAR; f-Q product; Stress generator

## I. INTRODUCTION

The new generation of quantum technology based on defects in semiconductor systems has many advantages over traditional systems. They can easily be integrated with both the solid-state electronics and optical systems paving way for highly integrated quantum-computing and quantum-sensing applications and technology. These defect based systems have quantum spin states which are traditionally controlled using magnetic fields. These magnetic field based systems can be bulky as they need both AC and DC magnetic field which needs integration of magnetic materials with semiconductor systems. Alternatives to magnetic fields based control of quantum spin-defect systems are electric fields, optical fields, and mechanical lattice vibrations. All these technologies not only facilitate close integration but also open avenues for new quantum-sensing systems. The mechanical lattice vibration based spin-state control system which relies on direct spin-phonon coupling, has attracted interest particularly in Nitrogen-vacancy (NV) center spins in diamond. Significant progress in integrating NV centers with MEMS has paved the way for studies of spins coupled to mechanical resonators [1-3].

MacQuarrie et al. [1,2] have demonstrated acoustically mediated spin-state control of nitrogen-vacancy centers in diamond. They further demonstrated complete coherent control by driving Rabi oscillations between  $|+1\rangle$  and  $|-1\rangle$  spin states. Similar di-vacancy based spin-defects have also been observed in SiC [3]. With ease of wafer scale integration of SiC on Si these quantum technologies have capabilities for developing solid-state wafer-scale hybrid quantum systems. Interrogating and controlling the di-vacancy spins in SiC with mechanical resonator can be achieved through use of an HBAR.

This is similar to the system that was implemented in experiments by MacQuarrie et al [1,2]. For understanding the limits of HBAR as a stress generator in SiC and diamond and compare it to silicon we fabricated HBARS on SiC, diamond and silicon substrates. We then measured quality factor as a function of temperature from 80K to room temperature at multiple resonant frequencies for each sample. The quality factors measured were then used to estimate the maximum stress generated at an anti-node inside the wafer using a 1D analytical model of an HBAR. We discovered that the maximum stress generated in the HBAR doesn't increase linearly with the quality factor and were able to verify this saturation of stress for with Comsol simulations. From our measurements and analysis we note that HBARS on SiC has tremendous potential for generating stress at GHz frequencies and hence playing an active role in the new generation of hybrid quantum sensors and systems.

## II. DEVICE FABRICATION

HBARS are comprised of thin film piezoelectric materials like AlN or ZnO sandwiched between metal electrodes which are solidly mounted on low acoustic loss substrates. Using the piezoelectric effect, high frequency overtones of the thickness mode generating high amplitude stress waves are transduced in the substrate. The fabrication process flow for HBARS is different for silicon, SiC and diamond. This is because of the varying substrate sizes. HBARS on silicon and SiC are fabricated on wafer scale substrates while HBARS on diamond are fabricated on chips which are 3mm×3mm in dimension. As the chips are small we cannot use the same process on all three substrates.

### A. Fabrication of HBARS on Silicon and SiC

Silicon and SiC being ubiquitous semiconductor materials are readily available in wafer sizes. Silicon HBARS were fabricated on 4 inch, 500μm thick, <100> oriented double side polished high resistivity substrates. In fabricating SiC HBARS we used double side polished 8° of <1120> 3 inch wafers. This unique orientation of SiC wafer was used as it is most efficient for coupling Z directional acoustic stress with the spin di-vacancies observed in 4H polytype of SiC. The fabrication process for HBARS in silicon and SiC is shown in Fig. 1.

### B. Fabrication of HBARS on Diamond

The diamond substrate used in making HBARS is a 300μm thick chip, oriented along <100> direction. These chips are commercially available single crystal type IIA CVD grown

diamonds from element six corporation. Because the diamond surface is nonconductive, bottom platinum electrode can be directly sputtered on the surface without a need of a spacer like silicon nitride. The diamond HBARs also use ZnO as the piezoelectric layer because the yield and uniformity of AlN on diamond chips was poor. HBARs were fabricated on diamond using the process shown in Fig. 2. Final fabricated devices with substrate sizes and material stack are shown in Fig. 3.

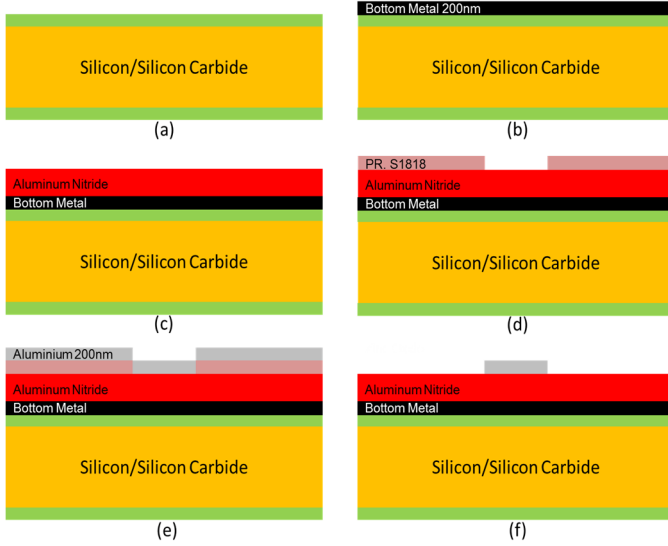


Fig. 1. Fabrication process flow for HBARs on silicon and SiC substrate: (a) 200nm thick low stress silicon nitride is grown on the DSP wafers by LPCVD. (b) 200nm thick bottom metal, Pt for silicon and Mo for SiC, is sputtered. The orientation of bottom metal is important to get highly orientated C axis AlN piezoelectric layer. (c) 1.5μm thick AlN is deposited by reactive-ion sputtering at 400°C. Rocking curve measurements are performed to ensure the AlN has good piezoelectric properties. (d) Photo resist mask is used for patterning the top electrode of Al on the AlN. As AlN is sensitive to TMAH, the developer options available are limited to soft developer like CD-30, which work efficiently with positive photo resist like S1818. (e) 200nm thick Aluminum top metal is evaporated using ebeam. Al being light weight is the preferred material for top electrode. (f) Al is then patterned using liftoff for defining the top electrode.

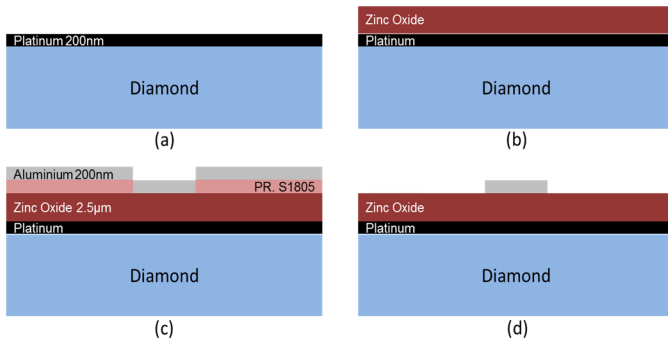


Fig. 2. Fabrication process flow for HBARs on diamond: (a) 200nm thick Platinum is sputtered as the bottom metal directly on the diamond surface. (b) 2.5μm thick ZnO is then reactive-ion sputtered on the bottom platinum electrode. Rocking curve measurements are performed to ensure ZnO has good piezoelectric performance. (c) S1805 photo resist is spray coated on the diamond chip and is then patterned using contact lithography. Spray coating is necessary as the diamond chips are 3mm×3mm in size and hence there are issues with spinning uniform thickness of resist. (d) 200nm thick aluminum is ebeam evaporated and then patterned by liftoff to define the top electrode.

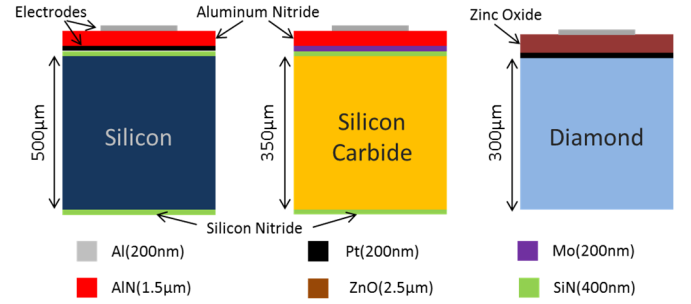


Fig. 3. Device geometries and material stacks for HBARs fabricated on silicon, SiC and diamond substrates.

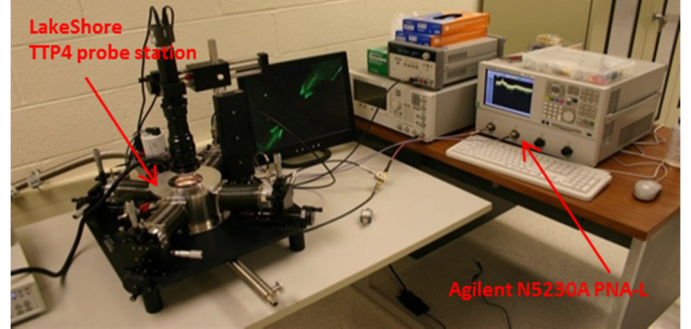


Fig. 4. Device characterization setup comprising of LakeShore probe station and Agilent network analyzer.

### III. DEVICE MEASUREMENT AND EXPERIMENTAL RESULTS

HBAR devices are measured as one port devices with the top electrode being the signal port and the bottom electrode acting as the ground plane. The characterization setup for HBARs shown in Fig. 4 consists of a LakeShore vacuum probe station with the capability to accurately control the temperature of the device under test from 80K to 295K and an Agilent N5230A parametric network analyzer. During the measurement, cable and probe parasitics were de-embedded from measured signal using calibration substrates. S11 measurements were performed on circular shaped HBARs of radius 250μm fabricated on SiC and diamond substrates and of radius 75μm fabricated on silicon substrate. The quality factor of multiple resonances for each of the substrate was measured as a function of device temperature using the Q circle method developed by Feld et al. [4]. The product of frequency and the measured quality factor (f-Q products) were then calculated for multiple resonant frequencies observed on each substrate. In SiC we measured the quality factor of resonances at 592MHz, 1.1 GHz, 3.2GHz and 3.4 GHz. The f-Q products of these resonances are shown in Fig. 5 as blue stars. In diamond HBARs we measured the f-Q products of resonances at 530MHz and 1.45GHz, which are shown in Fig. 5 as green circles. f-Q products measured at 1GHz, 2.23GHz and 3.02GHz for silicon HBARs are shown in Fig. 5 as red squares. Fig. 5 also shows the room temperature theoretical phonon-phonon damping dependent limits on the f-Q products as lines adopted from work by Tabrizian et al. [5]. Akheiser and Landau-Rumer damping which are the two major loss mechanisms form two different f-Q limited regions in Fig. 5. These regions separated by frequency are dependent upon the thermal phonon relaxation lifetimes in the materials.

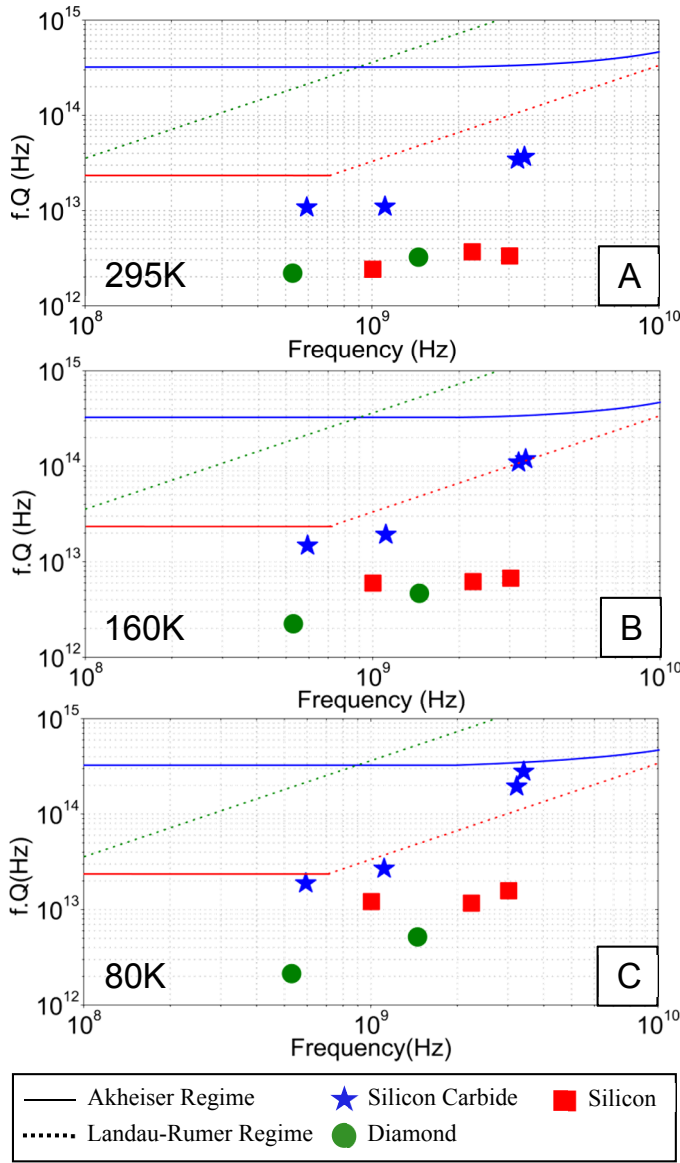


Fig. 5. Frequency-Quality factor product vs. Frequency graphs of HBAR resonances measured at temperatures 295K (plot A), 160K (plot B) and 80K (plot C). Data points on the plots represent measured resonances of silicon (red), diamond (green) and silicon carbide (blue) HBARs. The lines on the graph represent the two different phonon-phonon dissipation limited  $fQ$  values calculated for these materials at room temperature. In case of diamond we only see Landau-Rumer regime of damping as it has high thermal conductivity.

The  $fQ$  product for SiC was measured to be highest among the three materials at all the resonant frequencies.  $fQ$  product for SiC increases rapidly as temperature decreases compared to silicon and diamond. The measured  $fQ$  product for diamond at room temperature shown in Fig. 5A is about two orders of magnitude lower than the theoretically predicted values.  $fQ$  product of diamond also scales poorly with reducing temperature as compared to both silicon and SiC. To further compare how the Quality factor scales with temperature for all three materials we plot the measured Quality factor as function of temperature for one resonance in the Landau-Rumer regime of each of the substrates this is shown in Fig. 6. Fig. 6 also shows fits of quality factor vs. temperature trends to

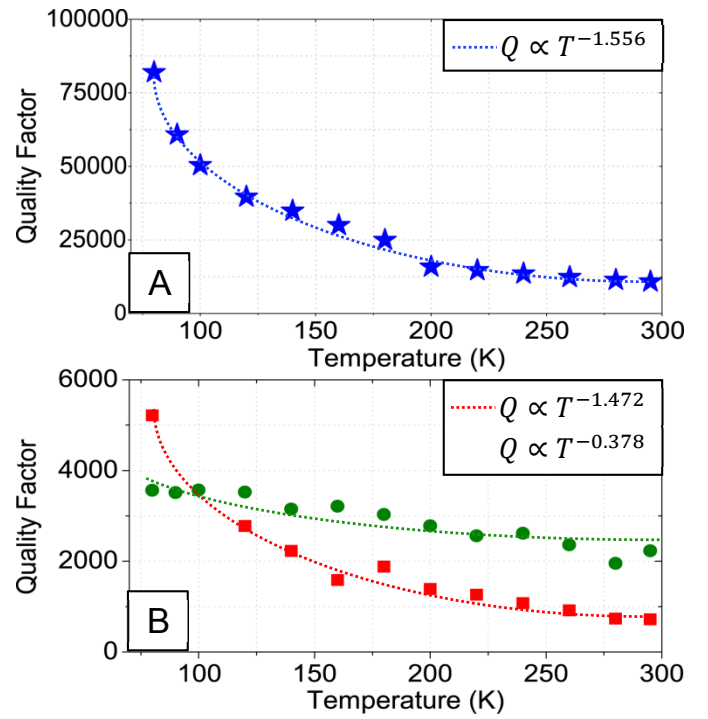


Fig. 6. Quality Factor v/s Temperature of A) 3.4GHz mode of SiC HBAR in blue, B) 3.02GHz mode of the silicon HBAR in red and 1.45GHz mode of the Diamond HBAR in green. The trendlines represent fits to  $Q \propto T^{-a}$  expression where  $T$  is the temperature. In plot A) the quality factor for SiC HBAR scales from 10800 at 295K to 82000 at 80K. In plot B) the quality factor from diamond HBAR scales from 2232 at 295K to 3564 at 80K. The quality factor for silicon HBAR scales from 720 at 295K to 5220 at 80K.

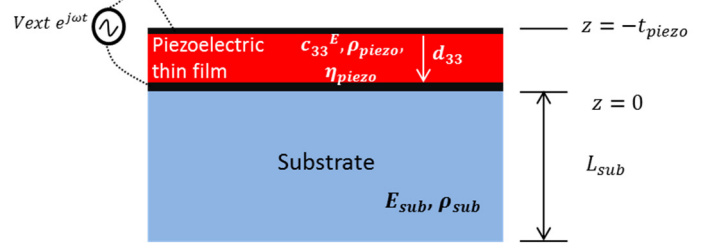


Fig. 7. Material properties and dimensions used for the analytical model of stress generated in HBAR.

expression  $Q \propto T^{-a}$ . Here the value of  $a$  is representative of the dominant loss mechanism limiting the quality factor of the resonator. For SiC HBAR and silicon HBAR from the fits to quality factor vs. temperature data value of  $a$  was calculated to be 1.556 and 1.472 respectively. This means that these resonators are partially anchor loss limited while operating in the Landau-Rumer regime. For the diamond HBAR the fit determined the coefficient to be 0.376 which means the dominant loss mechanism isn't anchor loss. We believe the quality factor of diamond HBAR is limited by the non-idealities of the diamond chip; particularly the top and bottom chip surfaces weren't perfectly parallel to each other thus forming a defective acoustic cavity in the HBAR and limiting the quality factor of the resonator. Hence the quality factor doesn't scale with the decreasing temperature as it did for silicon and SiC. To understand how quality factor and other material properties translate into the stress generated by HBAR we developed an analytical model described in section IV.

TABLE I. STRESS GENERATED BY HBAR FOR 1V DRIVE

HBAR Materials	Stress @ 295K	Stress @ 80K
Silicon -3.02GHz	2.20 MPa	2.90 MPa
Diamond -1.45GHz	1.43 MPa	1.51 MPa
Silicon Carbide -3.40GHz	4.05 MPa	6.15 MPa

## IV. MODEL FOR CALCULATING STRESS GENERATED BY HBAR

Mathematically we can calculate the stress generated in a HBAR along Z direction using 1D model for the piezoelectric transducer shown in Fig. 7 [6,7]. Longitudinal stress ( $T_z$ ) and displacement current ( $D_z$ ) due to Z directional strain developed due to potential ( $\phi$ ) across a piezoelectric layer are given by the constitutive equations (1) and (2). Where  $S_z$  the strain,  $E_z$  is the electric field,  $c_{33}$  is the stiffness coefficient,  $e_{33}$  is the piezoelectric coefficient and  $\epsilon_{33}$  is the dielectric permittivity of the piezoelectric layer. Behavior of the transducer can be modelled by the equation of motion shown in (3) for a Z directional displacement  $u_z$ . Where  $\eta_{piezo}$  is the damping which is inversely proportional to the quality factor ( $Q$ ) as shown in (4). Shown in (5),  $k_{33}^2$  accounts for the effect of the piezoelectric layer on the equation of motion. For solving the equation of motion we assume quasistatic condition and ignore the free carriers in the piezoelectric film. Taking  $\nabla \cdot D = 0$  of (2) and substituting in  $E_z = -\nabla \cdot \phi[z, t]$  we get (6) for  $z < 0$  in the piezoelectric layer.

$$T_z = c_{33}^E S_z + e_{33} d\phi/dz \quad (1)$$

$$D_z = \epsilon_{33}^E E_z + e_{33} S_z \quad (2)$$

$$\rho \frac{\partial^2 u_z}{\partial t^2} + \eta_{piezo} \frac{\partial u_z}{\partial t} = c_{33}^E (1 + k_{33}^2) \frac{\partial^2 u_z}{\partial z^2} = c_{33}^D \frac{\partial^2 u_z}{\partial z^2} \quad (3)$$

$$\eta_{piezo} = \rho_{piezo} \omega / Q \quad (4)$$

$$k_{33}^2 = e_{33}^2 / \epsilon_{piezo} c_{33}^E \quad (5)$$

$$\frac{\partial^2 \phi}{\partial z^2} = \frac{e_{33}}{\epsilon_{piezo}} \frac{\partial^2 u_z}{\partial z^2} \quad (6)$$

$$\phi[z, t] = \left\{ \frac{e_{33}}{\epsilon_{piezo}} u_1[z] + A1 z + A2 \right\} e^{j\omega t} \quad (7)$$

$$u_1[z] = C1 \sin(\gamma_{piezo} z) + C2 \cos(\gamma_{piezo} z) \quad (8)$$

$$u_2[z] = C3 \sin(\gamma_{sub} z) + C4 \cos(\gamma_{sub} z) \quad (9)$$

$$\gamma = \sqrt{(\rho \omega^2 - i\omega \eta / E)} \quad (10)$$

$$T_1[z] = c_{33}^D u_1'[z] + A1 e_{33} \quad (11)$$

$$T_2[z] = E_{sub} u_2'[z] \quad (12)$$

Equation (6) can be solved by assuming  $\phi[z, t]$  is of the form shown in (7), where  $A1$  and  $A2$  are constants and  $u_1[z]$  is the displacement in the piezoelectric layer. The displacements in the piezoelectric layer and the substrate are of the form of standing waves shown in (8) and (9) respectively. Where  $C1$ ,  $C2$ ,  $C3$  and  $C4$  are constants and  $\gamma$  is the wave number in the piezoelectric layer and substrate given by (10). Knowing the form of displacement we can calculate stress generated in the piezoelectric layer ( $T_1$ ) and in the substrate ( $T_2$ ) as shown in (11) and (12) respectively. For computing the stress generated, we calculate the values of the constants used in the equations namely  $A1$ ,  $A2$ ,  $C1$ ,  $C2$ ,  $C3$  and  $C4$  by applying boundary conditions to the free surfaces and interface of the piezoelectric and substrate layer. Solutions

to the differential equations are complex but do give us few insights in to the operation of HBAR as a stress generator. We observe that the stress is proportional to the amplitude of the drive signal and the stiffness of the substrate and scales linearly with it. The most non-intuitive insight is that the stress doesn't increase proportionally to the quality factor. We see in our simulations at low quality factors the stress increases linearly with the quality factor but then saturates as the value of quality factor becomes very large. This effect was also verified by doing Comsol simulations where we observed stagnation in amplitude of stress as quality factor was increased to large values. Plugging in the material properties, geometric sizes and the measured quality factors in the analytical model we calculated the maximum stress generated for various substrates as shown in Table I. From Table I it is clear that SiC leads the substrates as efficient stress generator with twice the amplitude of stress compared to silicon and thrice compared to diamond for same drive voltage of 1V.

## V. CONCLUSION

In conclusion, our study of f-Q and Q of acoustic modes in different semiconductors identified SiC HBAR as a clear winner as an efficient transducer for generating stress, especially at GHz frequencies. We also demonstrated a model for calculating the maximum stress generated by HBAR and show that the amplitude of stress is dependent on the quality factor and the stiffness coefficient of the material.

## ACKNOWLEDGMENT

The authors would like to thank the SRC and the Cornell Center for Material Research with funding from NSF MRSEC program (DMR- 1120296). This work was performed in part at the Cornell NanoScale Facility, a member of the NNCI, which is supported by the NSF (Grant ECCS-15420819). We also would like to thank Dr. Abram Falk and Prof. David Awschalom of University of Chicago for providing us SiC wafers and Dr. Amy Duwel of Draper Labs for discussions regarding HBARs.

## REFERENCES

- [1] E. R. MacQuarrie, T. A. Gosavi, N. R. Jungwirth, S. A. Bhawe, and G. D. Fuchs, "Mechanical spin control of nitrogen-vacancy centers in diamond," Phys. Rev. Lett., vol. 111, no. 22, p. 227602, 2013.
- [2] E. R. MacQuarrie, T. A. Gosavi, A. M. Moehle, N. R. Jungwirth, S. A. Bhawe, and G. D. Fuchs, "Coherent control of a nitrogen-vacancy center spin ensemble with a diamond mechanical resonator," Optica, vol. 2, no. 3, pp. 233-238, Mar. 2015.
- [3] A. L. Falk, P. V. Klimov, B. B. Buckley, V. Ivády, I. A. Abrikosov, G. Calusine, W. F. Koehl, Á. Gali, and D. D. Awschalom, "Electrically and mechanically tunable electron spins in silicon carbide color centers," Phys. Rev. Lett., vol. 112, no. 18, p. 187601, 2014.
- [4] D. A. Feld, R. Parker, R. Ruby, P. Bradley, and D. Shim, "After 60 years: a new formula for computing quality factor is warranted," Ultrasonics 2008, pp. 431-436.
- [5] R. Tabrizian, M. Rais-Zadeh, and F. Ayazi, "Effect of phonon interactions on limiting the f-Q product of micromechanical resonators," Proc. Transducers 2009, pp. 2131-2134.
- [6] K. F. Graff, Wave Motion in Elastic Solids. New York: Dover, 1991.
- [7] S. Ardanuc, A. Lal, "Two-port electromechanical model for bulk-piezoelectric excitation of surface micromachined beam resonators," IEEE JMEMS, vol. 18, no. 3, pp. 626-640, June 2009.